Water Research 86 (2015) 17–24

Contents lists available at ScienceDirect

Water Research

journal homepage: www.elsevier.com/locate/watres

Enhanced visible-light-driven photocatalytic inactivation of *Escherichia coli* using g-C_3N_4/TiO_2 hybrid photocatalyst synthesized using a hydrothermal-calcination approach

Guiying Li [a], Xin Nie [a, e], Jiangyao Chen [a], Qi Jiang [a, e], Taicheng An [a, *], Po Keung Wong [b], Haimin Zhang [c], Huijun Zhao [c], Hiromi Yamashita [d]

[a] State Key Laboratory of Organic Geochemistry and Guangdong Key Laboratory of Environmental Protection and Resources Utilization, Guangzhou Institute of Geochemistry, Chinese Academy of Sciences, Guangzhou 510640, China
[b] School of Life Sciences, The Chinese University of Hong Kong, Shatin, NT, Hong Kong SAR, China
[c] Centre for Clean Environment and Energy, Griffith University, Gold Coast Campus, QLD, 4222, Australia
[d] Division of Materials and Manufacturing Science, Graduate School of Engineering, Osaka University, 2-1 Yamadaoka, Suita, Osaka 565-0871, Japan
[e] University of Chinese Academy of Sciences, Beijing 100049, China

ARTICLE INFO

Article history:
Received 5 February 2015
Received in revised form
22 May 2015
Accepted 27 May 2015
Available online 4 June 2015

Keywords:
Water disinfection
Photocatalytic inactivation
g-C_3N_4/TiO_2
Escherichia coli K-12
Visible light irradiation

ABSTRACT

Biohazards are widely present in wastewater, and contaminated water can arouse various waterborne diseases. Therefore, effectively removing biohazards from water is a worldwide need. In this study, a novel visible-light-driven (VLD) graphitic carbon nitride (g-C_3N_4)/TiO_2 hybrid photocatalyst with high photocatalytic bacterial inactivation activity was successfully synthesized using a facile hydrothermal-calcination approach. The optimum synthesized hybrid photocatalyst is composed of micron-sized TiO_2 spheres (average diameter: *ca.* 2 μm) and wrapped with lamellar g-C_3N_4 (thickness: *ca.* 2 nm), with narrowing bandgap (*ca.* 2.48 eV), leading to a significant improvement of visible light (VL) absorption and effective separation of photo-generated electron–hole pairs. This greatly enhances VL photocatalytic inactivation activity towards bacteria in water. Using this hybrid photocatalyst, 10^7 cfu mL^{-1} of *Escherichia coli* K-12 could be completely inactivated within 180 min under VL irradiation. SEM images indicate that bacterial cells were greatly damaged, leading to a severe leakage of intracellular components during photocatalytic inactivation processes. The study concludes that bacterial cell destruction and water disinfection can be achieved using this newly fabricated VLD hybrid photocatalyst.

1. Introduction

With increasing populations and uncertain global climate changes, fresh water shortages require increased water recycling and reuse (Rodriguez et al., 2009; Rietveld et al., 2011; Chowdhury and Al-Zahrani, 2013; Haaken et al., 2014). Biohazards such as bacteria, viruses, and fungi are widely presented in wastewater, however, can cause a variety of diseases to humans and animals (Dorevitch et al., 2012; Dobrowsky et al., 2014; Soller et al., 2014). Unfortunately, conventional water disinfection methods, including chlorination, ozone, and ultraviolet (UV), have some disadvantages. For example, a number of biohazards are naturally resistant to traditional UV and chlorination treatments (Eischeid et al., 2011; Anastasi et al., 2013); the toxic and corrosive characteristics of ozone hinder its practical application (AWWA, 1995); the formation of disinfection byproducts, with potential carcinogenicity, is additional drawbacks of chlorination (Parker et al., 2014; Sharma et al., 2014). As such, effectively removing biohazards from water is a challenge that has received sustained attention (Wang et al., 2011a; Kubacka et al., 2014; Sun et al., 2014; Xiong et al., 2015), and versatile new technologies are highly desirable to simultaneously inactivate biohazards and eliminate disinfection debris.

Semiconductor titanium dioxide (TiO_2) photocatalysis has been recognized as a promising technology to purify wastewater containing a wide array of organic contaminants. It also can inactivate pathogenic microorganisms effectively, due to its superior photocatalytic oxidation ability, nontoxic and stable characteristics (Ruales-Lonfat et al., 2014; Santaella et al., 2014; An et al., 2015; Li

* Corresponding author.
E-mail address: antc99@gig.ac.cn (T. An).

http://dx.doi.org/10.1016/j.watres.2015.05.053
0043-1354/

et al., 2015). However, due to its wide band gap (the band gap generally refers to the energy difference between the top of the valence band (VB) and the bottom of the conduction band (CB) in semiconductors), TiO_2 photocatalysis is applied exclusively using UV light at $\lambda < 380$ nm. As such, much effort has been invested in synthesizing novel photocatalysts with a visible light response.

More recently, polymer-like semiconductors, such as graphitic carbon nitride (g-C_3N_4) and its hybrids, have been successfully synthesized using a facile thermal polycondensation method (Wang et al., 2009; Su et al., 2010; Zhang et al., 2010; Ge et al., 2012). The delocalized conjugated π structures in g-C_3N_4 have been found to lead to rapid photo-induced charge separation and a relatively slow charge recombination (Wang et al., 2011b). Furthermore, its relatively narrow band gap originating from the tri-s-triazine units connected with planar amino groups leads to efficient light harvesting within the visible light region and electric conductivity (Zhang et al., 2010). Given the advantages discussed above, it may be feasible to synthesize a heterojunction photocatalyst with broadened light response range, and to enhance photocatalytic activity under visible light irradiation, by combining π structures of g-C_3N_4 with highly active TiO_2. To date, most reports on g-C_3N_4 focus mainly either on energy application (Ong et al., 2015; Zuluaga et al., 2015), or organic pollutant elimination (Zhang et al., 2014; Munoz-Batista et al., 2015). Limited studies have explored the photocatalytic activity to inactivate bacteria using g-C_3N_4 (Huang et al., 2014), atomic single layer g-C_3N_4 (Zhao et al., 2014) and graphene and g-C_3N_4 nanosheets cowrapped elemental α-sulfur (Wang et al., 2013). However, no study has demonstrated the inactivation of bacteria in water using a g-C_3N_4/TiO_2 hybrid photocatalyst.

In this study, a visible-light-driven (VLD) hybrid photocatalyst comprised of g-C_3N_4 and TiO_2 was successfully synthesized using a facile hydrothermal-calcination approach. *Escherichia coli* K-12 (*E. coli* K-12, a Gram-negative bacterium) was chosen as the model biohazard in water to evaluate the photocatalytic inactivation activity. The morphological change of *E. coli* K-12, as well as bacterial destruction during the photocatalytic processes, was investigated to assess this potential of the hybrid catalyst to enhance photocatalytic bacterial inactivation.

2. Experimental section

2.1. Synthesis

The g-C_3N_4/TiO_2 hybrid photocatalysts with visible light response were synthesized using a facile hydrothermal-calcination approach. In a typical process, 1.0 g NH_4F and 1.0 g melamine were dispersed into 40 mL deionized water, and exposed to ultrasonic waves for 30 min. The mixtures were then transferred into 100 mL Teflon-line autoclaves with clean Ti foils (99.6% purity, $50 \times 25 \times 0.16$ mm) (Nie et al., 2013), and treated hydrothermally at 150 °C for 72 h in an oven. After the hydrothermal reaction, the resultant precipitates were collected using a centrifuge, washed thoroughly with distilled water, dried at 80 °C, and finally heated. The heating occurred at 550 °C in alumina crucibles sealed with aluminum foil in a muffle furnace for 4 h with a heating rate of 20 °C min^{-1}. For comparison, the pure TiO_2 was prepared without adding melamine at 1.0 g NH_4F at a hydrothermal temperature of 150 °C for 72 h; the pure g-C_3N_4 was synthesized by directly heating melamine using an identical heating procedure.

2.2. Characterization

The crystal phase composition and crystallinity characteristics of the samples were determined using a X-ray diffraction diffractometer (XRD, Rigaku D/MAX-2200 VPC). The surface morphologies of the synthesized photocatalysts were observed using a Field Emission Scanning Electron Microscope (FESEM, JEOL JSM-6330F) and transmission electron microscope (TEM, JEM-2010). X-ray photoelectron spectroscopy (XPS) was carried out using a Thermo ESCALAB250 spectrometer using a monochromated Al Kα (1486.6 eV) source operated at 110 W. Nitrogen adsorption and desorption isotherms as well as pore diameter distribution were recorded using a nitrogen adsorption apparatus (Micromeritics ASAP 2020 system). The Fourier transform infrared spectroscopy (FT-IR) spectra were investigated with a Bruker EQUINOX 55 spectrometer. UV–vis absorption spectra were recorded on a Shimadzu UV-2501PC.

2.3. Photocatalytic bactericidal activity evaluation

E. coli K-12 was chosen as the model bacteria to evaluate the visible light photocatalytic inactivation efficiency of the prepared photocatalysts. The photocatalytic inactivation experiments were carried out in an open Pyrex reactor (110 mL) with a double-walled cooling-water jacket to keep the solution temperature constant (25 ± 1 °C) throughout the experiments. The bacterial cells were firstly cultured in nutrient broth growth medium at 37 °C for 16 h with shaking, and then harvested by centrifugation at 4000 rpm for 15 min. The bacterial pellets were then washed with sterilized saline (0.9% NaCl) solution three times in a centrifuge and re-suspended in a sterilized saline solution to obtain suitable concentration of *E. coli* (10^7 colony-forming units per mL (cfu mL^{-1})). Before each experiment, the reactor was washed several times with a sterilized saline solution to remove the residual debris generated by bacterial decomposition. Then, 30 mg of the prepared photocatalyst was added into 50 mL solution containing 10^7 cfu mL^{-1} bacterial suspension. The reaction solution was kept at approximately 25 °C and stirred with a magnetic stirrer throughout the experiment. Before switching on a 300 W Xe lamp ($\lambda > 420$ nm with an UV filter, light intensity: 30 mW cm^{-2}; the spectrum of the Xenon lamp with the UV filter is shown in Fig. S1), dark adsorption was allowed for 30 min to establish an adsorption–desorption equilibrium. Then, at different time intervals, inactivation solution samples were collected and uniformly spread 0.1 mL of solution on nutrient agar plates (3 plate repeats per sample) after serial dilutions using the sterilized saline solution. The plates were incubated at 37 °C for 24 h to determine the viable cell count. The bacterial inactivation data reported in this paper are the average values obtained from experiments replicated in triplicate.

2.4. Preparation procedure for bacterial SEM study

Before and after inactivation, SEM was used to observe the destruction process of *E. coli* K-12 cells. The SEM sample preparation procedure was similar to the description in our previous work (Li et al., 2013; Sun et al., 2014); details can be found in the supporting information.

3. Results and discussion

3.1. Structural and optical characterizations of g-C_3N_4/TiO_2 hybrid photocatalyst

The structural and optical characterizations of the photocatalysts prepared in different conditions (different hydrothermal temperature, the amount of NH_4F and hydrothermal time) are provided in supporting information in Figs. S2–S8. An optimized g-C_3N_4/TiO_2 hybrid photocatalyst was obtained using 1.0 g NH_4F, 1.0 g melamine and a piece of Ti foil; these underwent hydrothermal

reaction at a temperature of 150 °C for 72 h, with post-calcination treatment. As Fig. 1a shows, the characteristic diffraction peaks of the XRD pattern for the hybrid photocatalyst were as follows: $2\theta = 25.3°$, 37.8°, 48.0°, 54.0°, 55.3°, 62.4° and 68.7° are attributed to {101}, {004}, {200}, {105}, {211}, {204}, and {112} planes of anatase TiO_2. The peak of 27.4° can be indexed to the (002) peak of g-C_3N_4 with an interlayer distance of 0.336 nm (Wang et al., 2009; Yan et al., 2010a), revealing that the hybrid photocatalyst consisted of both anatase TiO_2 and g-C_3N_4.

Fig. 1b shows the SEM images of the hybrid photocatalyst. Non-transparent lamellar g-C_3N_4, micron-sized TiO_2 spheres with a diameter of *ca.* 2 μm are observed. A few g-C_3N_4 hollow nanospheres and nanorods with open ends are also observed in the hybrid photocatalyst (Fig. S9), likely due to the rolling of lamellar g-C_3N_4 driven by the surface tension. Furthermore, the hybrid sample appears fluffier than pure g-C_3N_4 or TiO_2 with the same weight (Fig. 1c). This may be due to the curled g-C_3N_4 enhancing the g-C_3N_4/TiO_2 pore structure and surface area. TEM imagery further verifies that the sample consists of micron-sized spherical flocculent anatase TiO_2 wrapped with *ca.* 2 nm thickness of lamellar texture of g-C_3N_4 (Fig. 1d). The corresponding selected-area electron diffraction pattern, recorded from the red circled area, shows that the TiO_2 microspheres are polycrystalline (upper left inset in Fig. 1d). The corresponding high-resolution TEM image (lower left

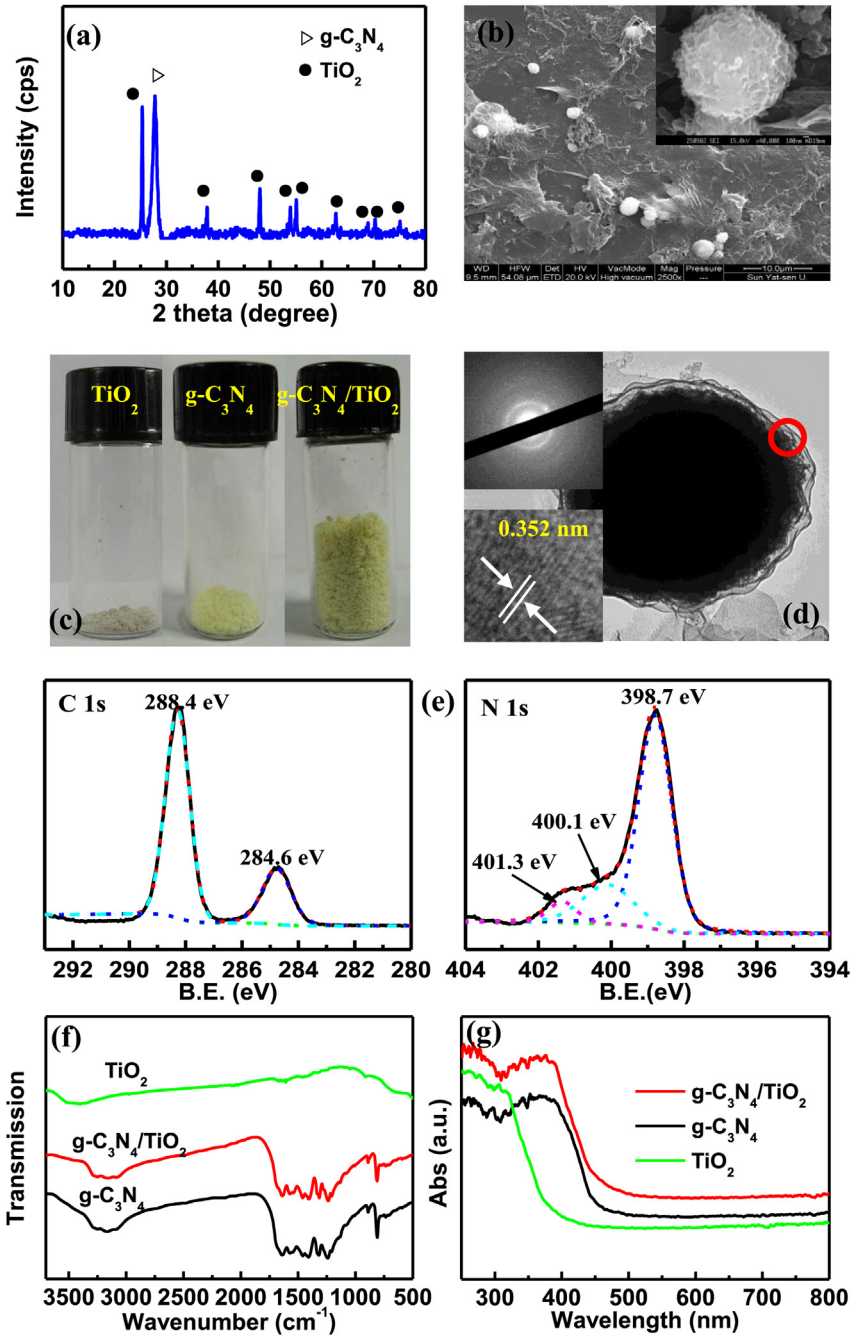

Fig. 1. (a) XRD pattern and (b) SEM image of hybrid photocatalyst; (c) The photograph of a volume comparison of 50 mg powder of TiO_2, g-C_3N_4, and g-C_3N_4/TiO_2; (d) TEM image and (e) XPS spectra of g-C_3N_4/TiO_2; (f) FT-IR spectra of TiO_2, g-C_3N_4 and g-C_3N_4/TiO_2; (g) UV–vis diffuse-reflectance spectra of TiO_2, g-C_3N_4 and g-C_3N_4/TiO_2.

inset in Fig. 1d) confirms that the lattice fringes spacing of 0.352 nm is assigned to (101) plane of anatase TiO_2. This agrees with the XRD result that anatase TiO_2 attached via (101) crystal plane to g-C_3N_4 in the prepared photocatalyst.

The optical properties of the prepared hybrid photocatalyst were also investigated. XPS spectra show (Fig. 1e) that the hybrid photocatalyst is composed of the elements C, N, O, and Ti (The data of O and Ti are not shown). The C 1s, N 1s, Ti 2p and O 1s could be easily observed in the survey spectra (The data are not shown), and the content of C_3N_4 in the hybrid materials is about 85% (mass percent). The C 1s peaks at 284.6, and 288.4 eV are assigned to the C–C bond in the turbostratic CN structure, and C atoms bonded to N atoms inside the g-C_3N_4 structure, respectively (Zhou et al., 2011). The N 1s binding energy peak at 398.7 eV can be identified as C=N–C groups and O–Ti–N bonds; the peaks at 400.1 and 401.3 eV can be attributed to N-$(C)_3$ and C–N–H groups, respectively (Mitoraj and Kisch, 2008; Ge et al., 2012). These results confirm the presence of g-C_3N_4 and TiO_2 in the hybrid photocatalyst.

As Fig. 1f shows, observing similar FT-IR spectra of pure g-C_3N_4 and g-C_3N_4/TiO_2 hybrid photocatalyst again confirms the existence of g-C_3N_4 in the hybrid photocatalyst. Moreover, the peaks at 1200–1460 cm^{-1} can be attributed to the distinctive stretching vibration modes of C–N in aromatic CN heterocycles. The peaks from 1500 to 1700 cm^{-1} can be assigned to the stretching vibration modes of C=N or bending vibration of O–H. The broad peaks at 3000–3300 cm^{-1} can be assigned to the stretching vibration mode of H–N and C–H. The sharp peak at 810 cm^{-1} is the breathing mode of triazine units. These characteristics suggest that a large amount of amino, carboxyl, and hydroxyl groups exist in the hybrid photocatalyst (Wang et al., 2011b; Zhang et al., 2012). These organic functional groups form cross-linked connections and covalent bonds between g-C_3N_4 and TiO_2, strengthening their chemical interaction. This may be of significance to transfer carriers, and induce a synergetic effect to enhance visible light absorbance and photocatalytic activity (Mitoraj and Kisch, 2008; Yan et al., 2010b; Zhang et al., 2012).

Fig. 1g shows the UV–vis diffuse-reflectance spectra of the photocatalysts. Pure TiO_2 only shows light absorption within the UV region, while pure g-C_3N_4 demonstrates an obvious absorption in visible light region at an absorption edge of *ca.* 480 nm. As expected, the g-C_3N_4/TiO_2 hybrid photocatalyst shows an increased visible light absorption with a certain extent red-shift of the absorption edge to *ca.* 500 nm. This indicates the bandgap narrowing of hybrid photocatalyst. Based on UV–vis diffuse reflectance spectra, the estimated bandgaps are *ca.* 3.02, 2.58 and 2.48 eV for pure TiO_2, g-C_3N_4 and g-C_3N_4/TiO_2 hybrid photocatalyst, respectively. The hybrid photocatalyst possesses the narrowest bandgap, perhaps due to chemical bonding between TiO_2 and g-C_3N_4. This may lead to light utilization improvement and photocatalytic efficiency.

3.2. Photocatalytic inactivation of *E. coli*

The photocatalytic inactivation of *E. coli* was used to evaluate the visible light activity of hybrid photocatalysts, prepared at various conditions. For comparison, pure g-C_3N_4 and TiO_2 were used as control photocatalysts. As Fig. 2a shows, the bacterial population remains almost unchanged within 300 min under visible-light irradiation with or without TiO_2. When g-C_3N_4 is present, an approximately 6-log reduction of *E. coli* is achieved after 300 min visible light irradiation. This is because g-C_3N_4 can harvest photons within the visible light region to generate e^- and h^+, effectively inactivating bacteria, due to its small bandgap (Li et al., 2010; Cui et al., 2011).

As expected, g-C_3N_4/TiO_2 demonstrates the highest photocatalytic inactivation activity, and could completely inactivate 10^7 cfu mL^{-1} *E. coli* within 180 min under visible-light irradiation. The highest photocatalytic inactivation activity was seen with the hybrid photocatalyst fabricated at 150 °C (Fig. 2b). Further hydrothermal temperature increases or decreases could decrease photocatalytic inactivation efficiencies. For instance, a slightly higher photocatalytic inactivation efficiency than with pure g-C_3N_4 is

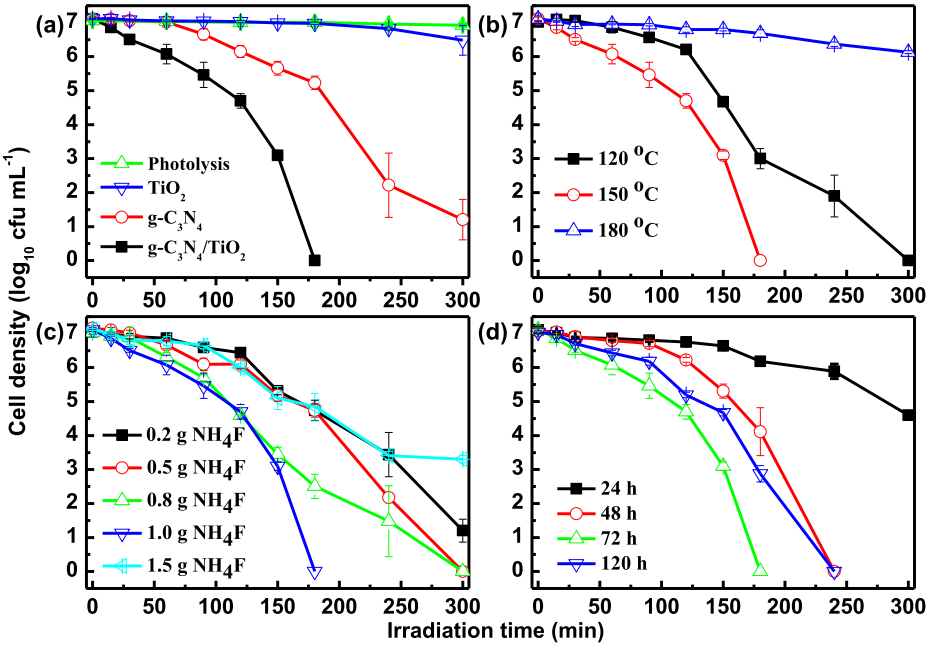

Fig. 2. Photocatalytic inactivation curves of *E. coli* K-12 under visible light irradiation using (a) TiO_2, g-C_3N_4, and g-C_3N_4/TiO_2; (b) g-C_3N_4/TiO_2 prepared with 1.0 g NH_4F and 72 h with different hydrothermal temperatures; (c) g-C_3N_4/TiO_2 prepared at 150 °C and 72 h with different NH_4F concentrations; (d) g-C_3N_4/TiO_2 prepared with 1.0 g NH_4F and 150 °C with different hydrothermal times.

obtained by the photocatalyst prepared at 120 °C. Only *ca.* 1-log of bacterial cells was inactivated within 300 min using the photocatalyst prepared at 180 °C.

Results revealed that the hydrothermal temperature could significantly affect photocatalyst properties and subsequently control photocatalytic activity. Fig. 2c shows the photocatalytic inactivation of *E. coli* by the hybrid photocatalysts, fabricated with different addition amounts of NH_4F. Approximately 6- and 7-log of *E. coli* are killed within 300 min by the catalysts prepared with 0.2 and 0.5 g NH_4F, respectively. By further increasing NH_4F to 1.0 g, the needed time to complete inactivate 10^7 cfu mL^{-1} of *E. coli* was shortened significantly to 180 min. However, increasing the added NH_4F to 1.5 g results in only 4-log of *E. coli* being inactivated within 300 min. Fig. 2d shows the photocatalytic inactivation efficiencies of *E. coli* using the photocatalysts, with different hydrothermal times. Only approximately 2-log of *E. coli* is killed within 300 min by the photocatalyst prepared at a hydrothermal time of 24 h, which is even lower than with pure g-C_3N_4 at the same inactivation time. For the catalysts hydrothermally treated for longer time, the needed time to completely inactivate bacterial cells was first shortened and then lengthened. When the hydrothermal time extends to 72 h, the obtained photocatalyst exhibits the highest inactivation ability, with complete inactivation achieved within 180 min. Combining these data with the photocatalyst characterization results, it appears that the prepared parameters have significant effects on the structural and optical properties of the resultant photocatalysts, affecting the visible light photocatalytic activity in the inactivation of *E. coli*.

3.3. Visible-light-driven photocatalytic inactivation mechanism

During the photocatalytic inactivation of bacteria process, various reactive species (RSs) may be produced and play different roles when g-C_3N_4/TiO_2 was used as catalyst. Therefore, different scavengers are used to remove specific RSs, to discriminate their contributions to the photocatalytic inactivation (Fig. 3). Isopropanol (10 mM) is used to scavenge $^{\bullet}OH$; $Na_2C_2O_4$ (10 mM) is used to quench h^+; and $K_2Cr_2O_7$ (50 μM) quenches the CB e^- (Fang et al., 2013). When no scavengers were added, 10^7 cfu mL^{-1} of *E. coli* could be completely inactivated within 180 min. When isopropanol was added, the photocatalytic inactivation efficiencies of *E. coli* only showed a small decrease, indicating a negligible contribution of $^{\bullet}OH$ to this photocatalytic bacteria inactivation system. However, the addition of $Na_2C_2O_4$ inhibits *E. coli* inactivation, and only approximately 0.5-log of cell density is inactivated. This indicates that h^+ rather than $^{\bullet}OH$ plays an important role in the photocatalytic bacteria inactivation in this system. The addition of $K_2Cr_2O_7$ could also reduce the inactivation efficiency of *E. coli* with a 5-log decrease in cell density, suggesting that the role of e^- is less than h^+ but higher than $^{\bullet}OH$. Both h^+ and e^- are the primary RSs of the catalyst when illuminated by the light; other RSs like $^{\bullet}OH$ from h^+, and $^{\bullet}O_2^-$ as well as H_2O_2 from e^-, could also be produced.

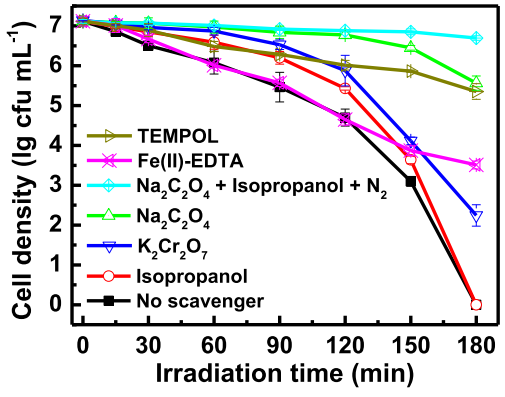

Fig. 3. Photocatalytic inactivation of *E. coli* K-12 with different scavengers by g-C_3N_4/TiO_2 hybrid photocatalyst prepared with 1.0 g NH_4F and hydrothermal temperature of 150 °C for 72 h.

To further ascertain the role of e^- in this system, a solution containing isopropanol and $Na_2C_2O_4$ degassed with N_2 is used to exclude all other species, except only reductive CB electrons. Only a slight decrease in the bacterial population was observed under this condition, suggesting that e^- from CB plays a very minor role in the photocatalytic process (Fang et al., 2013). This means that subsequently produced $^{\bullet}O_2^-$ or H_2O_2 from e^-, rather than the e^- itself, contributed to bacteria inactivation. To further determine the role of $^{\bullet}O_2^-$ and H_2O_2 during the photocatalytic inactivation process, 4-hydroxy-2,2,6,6-tetramethylpiperidinyloxy (TEMPOL, 2 mM) and Fe(II)-EDTA (10 μM) were used as scavengers, respectively (Fang et al., 2013; Shi et al., 2015). Only very slight decrease of photocatalytic inactivation efficiencies of *E. coli* was observed for the sample with addition of Fe(II)-EDTA, indicating the minor role of H_2O_2. In contrast, the bacterial inactivation was greatly restrained by the scavenger TEMPOL, suggesting the dominant role of $^{\bullet}O_2^-$ in this system. In summary, in this system, $^{\bullet}OH$ and H_2O_2 play a minor role in this photocatalytic inactivation, while h^+ and $^{\bullet}O_2^-$ are the main RSs for the inactivation of *E. coli*, directly attacking bacteria and leading to their decomposition (Yan et al., 2010a; Ge and Zhang, 2011).

Bacterial regrowth experiments were also conducted to further evaluate the photocatalytic bactericidal effectiveness of the hybrid photocatalyst g-C_3N_4/TiO_2 under visible light irradiation. After 3 h photocatalytic inactivation reaction, the solution was kept in the dark for another 96 h to allow bacterial self-repair. No surviving bacteria were detected, indicating that photocatalytic inactivation of *E. coli* by g-C_3N_4/TiO_2 for 3 h could cause irreparable bacterial damage. The *E. coli* destruction process using the g-C_3N_4/TiO_2 photocatalyst was also visually observed by SEM (Fig. 4). Before treatment, the *E. coli* cell had an intact cell structure and a well-preserved rod shape (Fig. 4a). During the inactivation process, the characteristic rod shape of the cell became abnormal, and the cell's shape is distorted (Fig. 4b–h). This points to cell damage, particularly for the cell membrane, which subsequently leads to severe leakage of intracellular components.

Potassium ion (K^+) is a crucial component in polysome and protein synthesis regulation, and is often used to evaluate cell membrane permeability. As Fig. 5 shows, along with cell death and cell structure destruction, K^+ concentration increases gradually as photocatalytic treatment time increases, indicating K^+ leakage from bacterial cells due to cell membrane permeability, leading to the loss of viability (Foster et al., 2011; Wu et al., 2011; Wang et al., 2012a). Further increasing the irradiation time to 5 h leads to even more severe morphological changes in the bacteria (Fig. 4h). The cell membrane is completely destroyed, along with severe leakage of intracellular contents. This suggests that the cell is completely inactivated and decomposed during the photocatalytic process by various RSs, especially h^+, $^{\bullet}O_2^-$ and H_2O_2 originating from the hybrid photocatalyst under visible light irradiation (Chen et al., 2011).

Based on the results above, the hybrid photocatalyst appears to demonstrate higher photocatalytic activity than pure g-C_3N_4 or TiO_2 alone under visible light irradiation. This suggests a synergistic effect between g-C_3N_4 and TiO_2 in the hybrid photocatalyst. As Fig. 6 shows, the photocatalytic activity is enhanced by effective photo-generated electron–hole pair separation. The g-C_3N_4 is photo-excited under visible light irradiation, to produce the separation of electrons in the lowest unoccupied molecular orbital

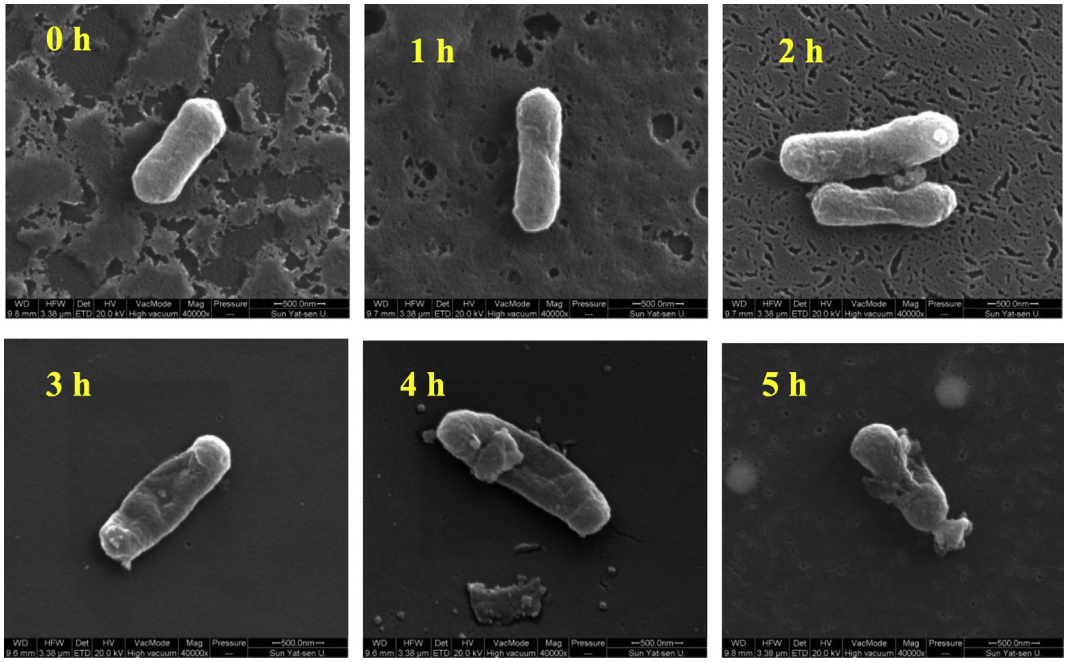

Fig. 4. SEM images of *E. coli* K-12 treated by g-C_3N_4/TiO_2 hybrid photocatalysts under visible light irradiation at different time.

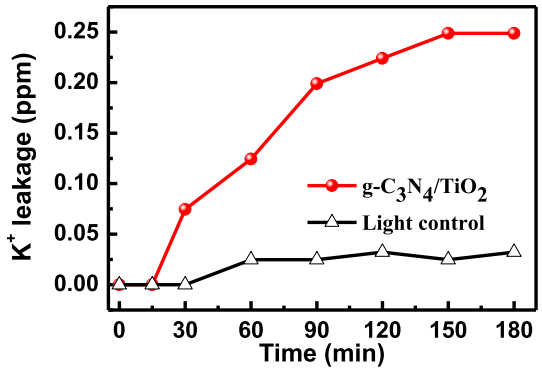

Fig. 5. Leakage of K^+ from *E. coli* K-12 cells (10^7 cfu mL^{-1}, 50 mL) under visible light irradiation alone (light control) and photocatalytic treatment with g-C_3N_4/TiO_2 at different times.

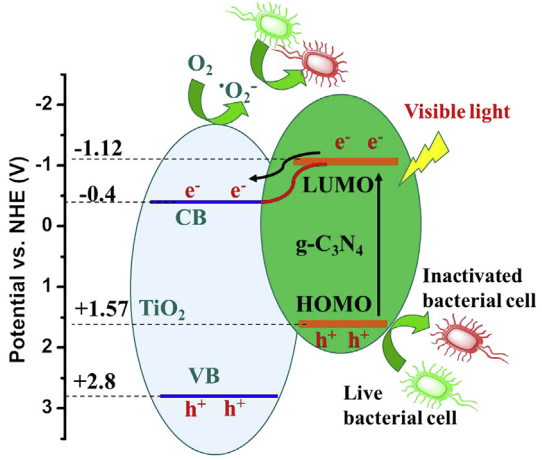

Fig. 6. Schematic diagram of the enhancement mechanism of g-C_3N_4/TiO_2 hybrid photocatalyst under visible light irradiation.

(LUMO) and the holes in the highest occupied molecular orbital (HOMO). The CB of TiO_2 (−0.40 V) is more positive than the LUMO of g-C_3N_4 (−1.12 V), while the VB of TiO_2 (+2.80 V) is lower than the HOMO of g-C_3N_4 (+1.57 V) (Zhou et al., 2011; Sun et al., 2012). As such, the photo-generated e^- could transfer efficiently from LUMO of photo-excited g-C_3N_4 to CB of TiO_2. This led to the accumulation of a large number of e^- and the formation of $^{\bullet}O_2^-$ and H_2O_2 via the scavenging e^- with adsorbed O_2 on the photocatalyst surface because the CB potential of TiO_2 (−0.40 V) was more negative than the standard redox potential $E^0(O_2/^{\bullet}O_2^-$, -0.33 V) and yielding $^{\bullet}O_2^-$ which then further reacted to finally produce H_2O_2 (Boonprakob et al., 2014). The suitable matching of CB and VB levels effectively promotes charge separation and suppresses the recombination of photo-generated e^- and h^+ pairs within the hybrid photocatalyst. As a consequence, the lifetime of photo-generated h^+ is prolonged, enhancing photocatalytic inactivation (Wang et al., 2012b). Nevertheless, the oxidation potential of HOMO of g-C_3N_4 is only +1.57 V, which can not directly oxidize adsorbed hydroxyl groups to generate $^{\bullet}OH$ (+2.70 V).

Thus, in this photocatalytic system, it appears only a very low concentration $^{\bullet}OH$ formed (Yan et al., 2010a), explaining why $^{\bullet}OH$ was not the major oxygen species in this inactivation process. Nevertheless, although the oxidation potential of the g-C_3N_4 HOMO (+1.57 V) is much lower than $^{\bullet}OH$ (+2.70 V), it is still high enough to decompose the cell membrane and kill the bacteria. Therefore, substantial interaction between g-C_3N_4 and TiO_2 in the hybrid photocatalyst is a vital prerequisite for the enhanced photocatalytic activity; this can subsequently increase the trapping of the photo-induced charge carriers, benefiting production of RSs. Furthermore, besides h^+, other RSs such as subsequently generated $^{\bullet}O_2^-$ and H_2O_2 can also attack biohazards, leading to efficient photocatalytic inactivation and completely decomposition of bacteria (Rengifo-Herrera et al., 2008; Zhou et al., 2011; Li et al., 2013).

4. Conclusions

The g-C_3N_4/TiO_2 hybrid photocatalyst with enhanced photocatalytic activity was successfully synthesized via a facile

hydrothermal-calcination method. The catalyst, comprised of micron-sized TiO_2 spheres wrapped with lamellar g-C_3N_4, significantly enhanced photocatalytic activity, inactivating bacteria under visible light irradiation. The enhancement was the result of a synergistic effect between g-C_3N_4 and TiO_2, which improved light absorption and the effective separation of photo-generated electron–hole pairs. Our results suggest that this new hybrid photocatalyst may facilitate water disinfection using visible light, particularly for purifying hospital wastewater contaminated with highly concentrated pathogenic microorganisms.

Acknowledgments

This is contribution No. IS–2064 from GIGCAS. This work was supported by National Natural Science Funds for Distinguished Young Scholars (41425015), NSFC (21077104 and 41373103), Research Grant Council, Hong Kong SAR Government (476811) and Earmarked Fund of SKLOG (SKLOG2011A02).

Appendix A. Supplementary data

Supplementary data related to this article can be found at http://dx.doi.org/10.1016/j.watres.2015.05.053.

References

An, T.C., An, J.B., Gao, Y.P., Li, G.Y., Fang, H.S., Song, W.H., 2015. Photocatalytic degradation and mineralization mechanism and toxicity assessment of antivirus drug acyclovir: experimental and theoretical studies. Appl. Catal. B Environ. 164, 279–287.

Anastasi, E.M., Wohlsen, T.D., Stratton, H.M., Katouli, M., 2013. Survival of *Escherichia coli* in two sewage treatment plants using UV irradiation and chlorination for disinfection. Water Res. 47, 6670–6679.

AWWA, 1995. Water Treatment: Principles and Practices of Water Supply Operations. American Water Works Association, Denver.

Boonprakob, N., Wetchakun, N., Phanichphant, S., Waxler, D., Sherrell, P., Nattestad, A., Chen, J., Inceesungvorn, B., 2014. Enhanced visible-light photocatalytic activity of g-C_3N_4/TiO_2 films. J. Colloid Interf. Sci. 417, 402–409.

Chen, Y.M., Lu, A.H., Li, Y., Zhang, L.S., Yip, H.Y., Zhao, H.J., An, T.C., Wong, P.K., 2011. Naturally occurring sphalerite as a novel cost-effective photocatalyst for bacterial disinfection under visible light. Environ. Sci. Technol. 45, 5689–5695.

Chowdhury, S., Al-Zahrani, M., 2013. Reuse of treated wastewater in Saudi Arabia: an assessment framework. J. Water Reuse Desalin 3, 297–314.

Cui, Y.J., Zhang, J.S., Zhang, G.G., Huang, J.H., Liu, P., Antonietti, M., Wang, X.C., 2011. Synthesis of bulk and nanoporous carbon nitride polymers from ammonium thiocyanate for photocatalytic hydrogen evolution. J. Mater. Chem. 21, 13032–13039.

Dobrowsky, P.H., De Kwaadsteniet, M., Cloete, T.E., Khan, W., 2014. Distribution of indigenous bacterial pathogens and potential pathogens associated with roof-harvested rainwater. Appl. Environ. Microbiol. 80, 2307–2316.

Dorevitch, S., Pratap, P., Wroblewski, M., Hryhorczuk, D.O., Li, H., Liu, L.C., Scheff, P.A., 2012. Health risks of limited-contact water recreation. Environ. Health. Persp 120, 192–197.

Eischeid, A.C., Thurston, J.A., Linden, K.G., 2011. UV disinfection of adenovirus: present state of the research and future directions. Crit. Rev. Environ. Sci. Technol. 41, 1375–1396.

Fang, H.S., Gao, Y.P., Li, G.Y., An, J.B., Wong, P.K., Fu, H.Y., Yao, S.D., Nie, X.P., An, T.C., 2013. Advanced oxidation kinetics and mechanism of preservative propylparaben degradation in aqueous suspension of TiO_2 and risk assessment of its degradation products. Environ. Sci. Technol. 47, 2704–2712.

Foster, H.A., Ditta, I.B., Varghese, S., Steele, A., 2011. Photocatalytic disinfection using titanium dioxide: spectrum and mechanism of antimicrobial activity. Appl. Microbiol. Biotechnol. 90, 1847–1868.

Ge, L., Zuo, F., Liu, J.K., Ma, Q., Wang, C., Sun, D.Z., Bartels, L., Feng, P.Y., 2012. Synthesis and efficient visible light photocatalytic hydrogen evolution of polymeric g-C_3N_4 coupled with CdS quantum dots. J. Phys. Chem. C 116, 13708–13714.

Ge, S.X., Zhang, L.Z., 2011. Efficient visible light driven photocatalytic removal of RhB and NO with low temperature synthesized In(OH)(x)S-y hollow nanocubes: a comparative study. Environ. Sci. Technol. 45, 3027–3033.

Haaken, D., Dittmar, T., Schmalz, V., Worch, E., 2014. Disinfection of biologically treated wastewater and prevention of biofouling by UV/electrolysis hybrid technology: influence factors and limits for domestic wastewater reuse. Water Res. 52, 20–28.

Huang, J.H., Ho, W.K., Wang, X.C., 2014. Metal-free disinfection effects induced by graphitic carbon nitride polymers under visible light illumination. Chem. Commun. 50, 4338–4340.

Kubacka, A., Diez, M.S., Rojo, D., Bargiela, R., Ciordia, S., Zapico, I., Albar, J.P., Barbas, C., dos Santos, V., Fernandez-Garcia, M., Ferrer, M., 2014. Understanding the antimicrobial mechanism of TiO_2-based nanocomposite films in a pathogenic bacterium. Sci. Rep. 4, 9.

Li, G.Y., Liu, X.L., An, T.C., Yang, H., Zhang, S.Q., Zhao, H.J., 2015. Photocatalytic and photoelectrocatalytic degradation of small biological compounds at TiO_2 photoanode: a case study of nucleotide bases. Catal. Today 242, Part B, 363–371.

Li, G.Y., Liu, X.L., Zhang, H.M., Wong, P.-K., An, T.C., Zhao, H.J., 2013. Comparative studies of photocatalytic and photoelectrocatalytic inactivation of *E. coli* in presence of halides. Appl. Catal. B: Environ. 140–141, 225–232.

Li, Y.G., Zhang, J.A., Wang, Q.S., Jin, Y.X., Huang, D.H., Cui, Q.L., Zou, G.T., 2010. Nitrogen-rich carbon nitride hollow vessels: synthesis, characterization, and their properties. J. Phys. Chem. B 114, 9429–9434.

Mitoraj, D., Kisch, H., 2008. The nature of nitrogen-modified titanium dioxide photocatalysts active in visible light. Angew. Chem. Int. Ed. 47, 9975–9978.

Munoz-Batista, M.J., Fernandez-Garcia, M., Kubacka, A., 2015. Promotion of CeO_2-TiO_2 photoactivity by g-C_3N_4: ultraviolet and visible light elimination of toluene. Appl. Catal. B Environ. 164, 261–270.

Nie, X., Chen, J.Y., Li, G.Y., Shi, H.X., Zhao, H.J., Wong, P.K., An, T.C., 2013. Synthesis and characterization of TiO_2 nanotube photoanode and its application in photoelectrocatalytic degradation of model environmental pharmaceuticals. J. Chem. Technol. Biotechnol. 88, 1488–1497.

Ong, W.J., Tan, L.L., Chai, S.P., Yong, S.T., 2015. Graphene oxide as a structure-directing agent for the two-dimensional interface engineering of sandwich-like graphene-g-C_3N_4 hybrid nanostructures with enhanced visible-light photoreduction of CO_2 to methane. Chem. Commun. 51, 858–861.

Parker, K.M., Zeng, T., Harkness, J., Vengosh, A., Mitch, W.A., 2014. Enhanced formation of disinfection byproducts in shale gas wastewater-impacted drinking water supplies. Environ. Sci. Technol. 48, 11161–11169.

Rengifo-Herrera, J.A., Mielczarski, E., Mielczarski, J., Castillo, N.C., Kiwi, J., Pulgarin, C., 2008. *Escherichia coli* inactivation by N, S co-doped commercial TiO_2 powders under UV and visible light. Appl. Catal. B Environ. 84, 448–456.

Rietveld, L.C., Norton-Brandao, D., Shang, R., van Agtmaal, J., van Lier, J.B., 2011. Possibilities for reuse of treated domestic wastewater in The Netherlands. Water Sci. Technol. 64, 1540–1546.

Rodriguez, C., Van Buynder, P., Lugg, R., Blair, P., Devine, B., Cook, A., Weinstein, P., 2009. Indirect potable reuse: a sustainable water supply alternative. Int. J. Environ. Res. Publ. Health 6, 1174–1209.

Ruales-Lonfat, C., Benitez, N., Sienkiewicz, A., Pulgarin, C., 2014. Deleterious effect of homogeneous and heterogeneous near-neutral photo-Fenton system on *Escherichia coli*. Comparison with photo-catalytic action of TiO_2 during cell envelope disruption. Appl. Catal. B: Environ. 160–161, 286–297.

Santaella, C., Allainmat, B., Simonet, F., Chaneac, C., Labille, J., Auffan, M., Rose, J., Achouak, W., 2014. Aged TiO_2-based nanocomposite used in sunscreens produces singlet oxygen under long-wave uv and sensitizes *Escherichia coli* to cadmium. Environ. Sci. Technol. 48, 5245–5253.

Sharma, V.K., Zboril, R., McDonald, T.J., 2014. Formation and toxicity of brominated disinfection byproducts during chlorination and chloramination of water: a review. J. Environ. Sci. Health B 49, 212–228.

Shi, H.X., Huang, G.C., Xia, D.H., Ng, T.W., Yip, H.Y., Li, G.Y., An, T.C., Zhao, H.J., Wong, P.K., 2015. Role of in situ resultant H_2O_2 in the visible-light-driven photocatalytic inactivation of *E. coli* using natural sphalerite: a genetic study. J. Phys. Chem. B 119, 3104–3111.

Soller, J.A., Schoen, M.E., Varghese, A., Ichida, A.M., Boehm, A.B., Eftim, S., Ashbolt, N.J., Ravenscroft, J.E., 2014. Human health risk implications of multiple sources of faecal indicator bacteria in a recreational waterbody. Water Res. 66, 254–264.

Su, F.Z., Mathew, S.C., Lipner, G., Fu, X.Z., Antonietti, M., Blechert, S., Wang, X.C., 2010. mpg-C_3N_4-catalyzed selective oxidation of alcohols using O-2 and visible light. J. Am. Chem. Soc. 132, 16299–16301.

Sun, H.W., Li, G.Y., Nie, X., Shi, H.X., Wong, P.K., Zhao, H.J., An, T.C., 2014. Systematic approach to in-depth understanding of photoelectrocatalytic bacterial inactivation mechanisms by tracking the decomposed building blocks. Environ. Sci. Technol. 48, 9412–9419.

Sun, J.X., Yuan, Y.P., Qiu, L.G., Jiang, X., Xie, A.J., Shen, Y.H., Zhu, J.F., 2012. Fabrication of composite photocatalyst g-C_3N_4-ZnO and enhancement of photocatalytic activity under visible light. Dalton. T. 41, 6756–6763.

Wang, P.H., Zhou, T., Wang, R., Lim, T.T., 2011a. Carbon-sensitized and nitrogen-doped TiO_2 for photocatalytic degradation of sulfanilamide under visible-light irradiation. Water Res. 45, 5015–5026.

Wang, W.J., Yu, J.C., Xia, D.H., Wong, P.K., Li, Y.C., 2013. Graphene and g-C_3N_4 nanosheets cowrapped elemental alpha-sulfur as a novel metal-free heterojunction photocatalyst for bacterial inactivation under visible-light. Environ. Sci. Technol. 47, 8724–8732.

Wang, W.J., Yu, Y., An, T.C., Li, G.Y., Yip, H.Y., Yu, J.C., Wong, P.K., 2012a. Visible-light-driven photocatalytic inactivation of *E. coli* K-12 by bismuth vanadate nanotubes: bactericidal performance and mechanism. Environ. Sci. Technol. 46, 4599–4606.

Wang, X.C., Maeda, K., Thomas, A., Takanabe, K., Xin, G., Carlsson, J.M., Domen, K., Antonietti, M., 2009. A metal-free polymeric photocatalyst for hydrogen production from water under visible light. Nat. Mater. 8, 76–80.

Wang, Y., Shi, R., Lin, J., Zhu, Y., 2011b. Enhancement of photocurrent and photocatalytic activity of ZnO hybridized with graphite-like C_3N_4. Energ. Environ. Sci. 4, 2922–2929.

Wang, Y., Wang, X.C., Antonietti, M., 2012b. Polymeric graphitic carbon nitride as a heterogeneous organocatalyst: from photochemistry to multipurpose catalysis

to sustainable chemistry. Angew. Chem. Int. Ed. 51, 68–89.
Wu, D.H., You, H., Jin, D.R., Li, X.C., 2011. Enhanced inactivation of *Escherichia coli* with Ag-coated TiO_2 thin film under UV-C irradiation. J. Photochem. Photobiol. A: Chem. 217, 177–183.
Xiong, L., Ng, T.W., Yu, Y., Xia, D.H., Yip, H.Y., Li, G.Y., An, T.C., Zhao, H.J., Wong, P.K., 2015. N-type Cu_2O film for photocatalytic and photoelectrocatalytic processes: its stability and inactivation of *E. coli*. Electrochim. Acta 153, 583–593.
Yan, S.C., Li, Z.S., Zou, Z.G., 2010a. Photodegradation of rhodamine B and methyl orange over boron-doped g-C_3N_4 under visible light irradiation. Langmuir 26, 3894–3901.
Yan, S.C., Lv, S.B., Li, Z.S., Zou, Z.G., 2010b. Organic-inorganic composite photocatalyst of g-C_3N_4 and TaON with improved visible light photocatalytic activities. Dalton. T. 39, 1488–1491.
Zhang, J.S., Zhang, G.G., Chen, X.F., Lin, S., Mohlmann, L., Dolega, G., Lipner, G., Antonietti, M., Blechert, S., Wang, X.C., 2012. Co-monomer control of carbon nitride semiconductors to optimize hydrogen evolution with visible light. Angew. Chem. Int. Ed. 51, 3183–3187.
Zhang, L., Jing, D.W., She, X.L., Liu, H.W., Yang, D.J., Lu, Y., Li, J., Zheng, Z.F., Guo, L.J., 2014. Heterojunctions in g-C_3N_4/TiO_2(B) nanofibres with exposed (001) plane and enhanced visible-light photoactivity. J. Mater. Chem. A 2, 2071–2078.
Zhang, Y.J., Mori, T., Ye, J.H., Antonietti, M., 2010. Phosphorus-doped carbon nitride solid: enhanced electrical conductivity and photocurrent generation. J. Am. Chem. Soc. 132, 6294–6295.
Zhao, H.X., Yu, H.T., Quan, X., Chen, S., Zhang, Y.B., Zhao, H.M., Wang, H., 2014. Fabrication of atomic single layer graphitic-C_3N_4 and its high performance of photocatalytic disinfection under visible light irradiation. Appl. Catal. B: Environ. 152, 46–50.
Zhou, X.S., Peng, F., Wang, H.J., Yu, H., Fang, Y.P., 2011. Carbon nitride polymer sensitized TiO_2 nanotube arrays with enhanced visible light photoelectrochemical and photocatalytic performance. Chem. Commun. 47, 10323–10325.
Zuluaga, S., Liu, L.H., Shafiq, N., Rupich, S.M., Veyan, J.F., Chabal, Y.J., Thonhauser, T., 2015. Structural band-gap tuning in g-C_3N_4. Phys. Chem. Chem. Phys. 17, 957–962.